IEEE Photonics Journal
An IEEE Photonics Society Publication

Open Access

Angular Random Walk Improvement of Resonator Fiber Optic Gyro by Optimizing Modulation Frequency

Volume 11, Number 4, August 2019

Wei Gao
Zhuo Wang
Guochen Wang
Weiqi Miao

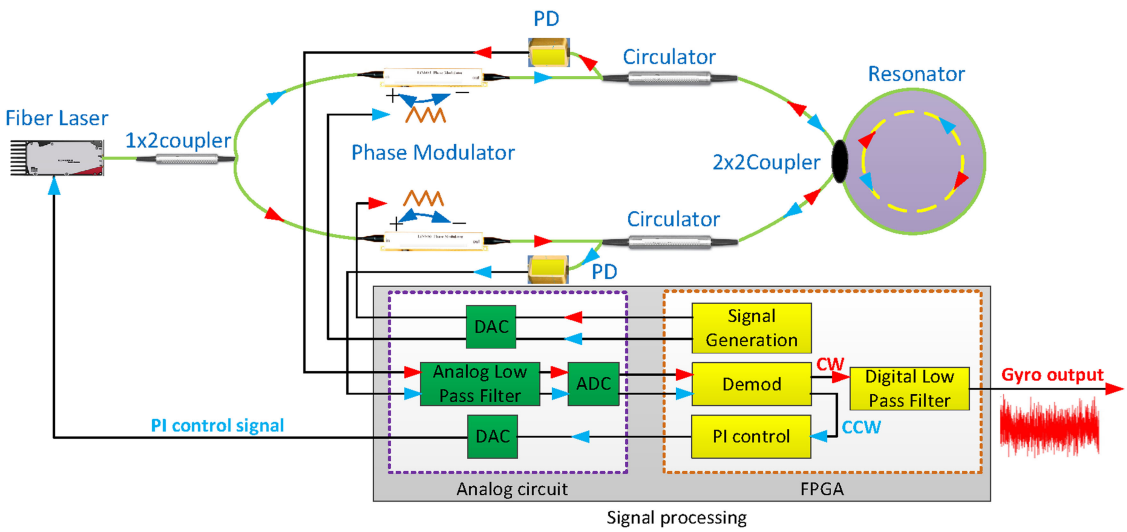

DOI: 10.1109/JPHOT.2019.2928458

Angular Random Walk Improvement of Resonator Fiber Optic Gyro by Optimizing Modulation Frequency

Wei Gao, Zhuo Wang, Guochen Wang, and Weiqi Miao

School of Instrument Science and Engineering, Harbin Institute of Technology, Harbin 150001, China

DOI:10.1109/JPHOT.2019.2928458

Manuscript received April 21, 2019; revised June 25, 2019; accepted July 10, 2019. Date of publication July 15, 2019; date of current version July 26, 2019. This work was supported in part by the National Natural Science Foundation of China under Grant 51709068, in part by the China Postdoctoral Science Foundation under Grant 2018M631920, and in part by the Postdoctoral Foundation of Heilongjiang Province Government under Grant LBH-Z17091. Corresponding author: Guochen Wang (e-mail: wanggc@hit.edu.cn).

Abstract: As a second-generation fiber optic gyro (FOG), the resonator fiber optic gyro (RFOG) has great potential in miniaturization and high-precision application. At present, white noises in the system have become important factors restricting the performance improvement of RFOG. For the first time, the shot noise, thermal noise, and relative intensity noise in the RFOG are analyzed and modeled, which are used to establish the angular random walk (ARW) model of RFOG. Based on the ARW model, an improvement method of ARW is proposed by adjusting the modulation frequency. In order to make this method effective, we use the particle swarm optimization algorithm to optimize the multi-parameter involved in ARW. Then, the experiment of optimizing modulation frequency is executed, which verifies that this method can effectively improve ARW and reduce the influence of white noises in RFOG.

Index Terms: Resonator fiber optic gyro, Angular random walk, Modulation frequency optimization, Particle swarm optimization.

1. Introduction

Gyro is an inertial device for measuring rotation velocity. Mechanical gyro, laser gyro, fiber optic gyro, and micro-optical gyro are widely applied in different fields [1]–[6]. Since its inception, fiber optic gyro (FOG) has been widely used in military and civilian fields due to its advantages of wide coverage, simple signal process and large dynamic range [4], [7]–[9].

Resonator fiber optic gyro (RFOG) is the second-generation FOG after interferometric fiber optic gyro (IFOG). RFOG greatly reduces the fiber length of resonator by utilizing multi-beam interference, which is useful for miniaturization and accuracy improvement of gyro [10]–[12]. At present, non-reciprocity errors and white noises in RFOG are two main factors limiting the performance improvement. There are many researches on non-reciprocity errors of RFOG and many achievements have been made [13]–[17]. However, currently there are few researches on white noise in RFOG. The optical components in FOG causes larger white noises [4], [18], [19]. The angular random walk (ARW) is the error coefficient of gyro accumulated by white noises, which is also an important factor for evaluating gyro performance like zero-bias stability and scale factor. Thus, it is important to improve ARW.

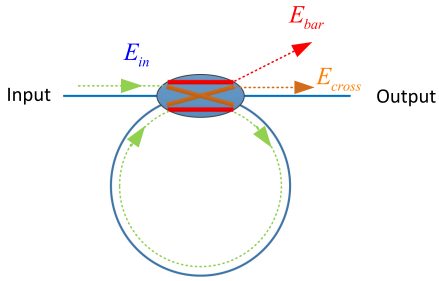

Fig. 1. Diagram of the resonator.

At present, the methods for improving the ARW of FOG are mostly applied in IFOG [20]. The errors caused by white noises are closely related to the signal detection and processing method. Therefore methods applied in IFOG to improve ARW are not applicable to RFOG. The white noises in RFOG mainly include the shot noise, thermal noise of the photodetector, relative intensity noise of the light source, and second-order backscattering. Although the ARW model that combines all of the above noises is currently not established, researchers have done some researches on one or several of these noises. Hu *et al*. analyzed the ARW model affected by Rayleigh backscattering, and the influence of resonator parameters on ARW [21]. RFOG and resonant micro-optical gyro (RMOG) have similarity in white noise analysis. Guillén-Torres *et al*. analyzed the amplitude noise of resonant micro-optical gyro, and established gyro standard deviation model for different noise components [22].

In this paper, the shot noise, thermal noise and relative intensity noise existing in the RFOG system are combined with signal processing to establish ARW model. Optimization method of modulation frequency is proposed for improving ARW. For the main system parameters involved in the ARW model, we first analyze their impacts on ARW respectively in different modulation frequencies. This step can only determine the approximate optimization range of each parameter, and cannot optimize the multi-parameter at the same time. Therefore, the particle swarm optimization (PSO) algorithm is introduced into the experiment for multi-parameter optimization. After other system parameters are optimized, the modulation frequency is changed to perform three sets of experiments. Through theoretical and experimental verification, reasonable setting of the modulation frequency can effectively improve the ARW, thereby improving the gyro performance.

2. Modeling

The error induced by white noise is related to the output intensity of resonator and the demodulation signal sensitivity. Therefore, in this part, we first establish the transfer model of the resonator, then establish the demodulation sensitivity model, and finally combine the two to derive the ARW model affected by white noises.

2.1 Resonator Transfer Model

According to Fig. 1, the incident light E_{in} enters resonator from the input port, and part of the energy recorded as E_{bar} passes through the red straight arm directly to output port. Another part of energy enters the resonator through brown coupling arm and transmits therein cyclically. When this part of light transmits to coupler each time, part of it will output through coupling arm, and the remaining energy continues to transmit in resonator. In this way, those light waves reaching the output port superimpose each other to form E_{cross}. E_{bar} passes through the straight arm only once without passing through the coupling arm. E_{cross} is superimposed by the light waves passing through the coupling arm, no matter how many times they pass through the coupling arm.

The light field of input port can be expressed as:

$$E_{in} = E_0 \exp j[\omega t + \phi(t)] \tag{1}$$

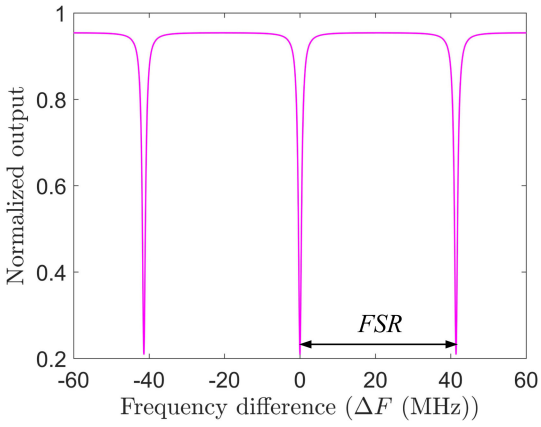

Fig. 2. Normalized output of resonator.

Where, E_0 is the amplitude of light field, ω is the angular frequency of light wave, and $\phi(t)$ is the randomly varying phase. According to the transmission principle, the output light field from the straight arm can be expressed as:

$$E_{bar} = \sqrt{1-k_c}\sqrt{1-\alpha_c}E_0 \exp j[\omega t + \phi(t)] \tag{2}$$

Where, k_c and α_c are coupling coefficient and loss coefficient of coupler. Light waves that pass through the coupling arm are superimposed on the output port, which can be expressed as:

$$\begin{aligned} E_{cross} = {} & k_c(1-\alpha_c)\sqrt{1-\alpha_L}E_0 \exp j(\omega t + \pi) \\ & \times \sum_{n=1}^{\infty} \left(\sqrt{1-k_c}\sqrt{1-\alpha_c}\sqrt{1-\alpha_L}\right)^{n-1} \exp j[\phi(t-n\tau) - \omega n\tau] \end{aligned} \tag{3}$$

α_L is the fiber loss of resonator including the splicing loss. n is the times of the light wave passing through resonator. τ is the transit time of light traveling one circle in resonator. At the output port, destructive interference occurs between E_{bar} and E_{cross}. To further simplify, the normalized output of resonator is:

$$H = \frac{|E_{bar}+E_{cross}|^2}{|E_0|^2} = (1-\alpha_c)\left[1 - \rho \cdot \frac{(1-Q)^2}{(1-Q)^2 + 4Q\sin^2(\pi\tau\cdot\Delta F)}\right] \tag{4}$$

Where, ΔF represents the frequency difference between the laser and resonant frequency of resonator, $\rho = 1 - \frac{1}{(1-\alpha_c)}[T^2 - \frac{2TR}{1-Q} + \frac{(R')^2}{1-(Q')^2}\frac{1+Q}{1-Q}]^2$. $T = \sqrt{1-k_c}\sqrt{1-\alpha_c}$ represents the loss coefficient when the light passes through the straight arm once. $R' = k_c(1-\alpha_c)\sqrt{1-\alpha_L}$ represents the loss coefficient that light couples into resonator traveling one circle and then couples to output port. $Q' = \sqrt{1-k_c}\sqrt{1-\alpha_c}\sqrt{1-\alpha_L}$ represents the loss coefficient of light transmitting in resonator for one cycle. Considering the effect of laser linewidth, R' and Q' can be rewritten: $R = k_c(1-\alpha_c)\sqrt{1-\alpha_L}e^{\delta f\tau}$, $Q = \sqrt{1-k_c}\sqrt{1-\alpha_c}\sqrt{1-\alpha_L}e^{\delta f\tau}$, δf is laser linewidth.

The Fig. 2 shows the normalized output of resonator according to Eq. (4). In the figure, FSR (free spectral range) represents the frequency spacing between two adjacent resonant valleys, which can be further defined as:

$$FSR = \frac{c}{n_{eff}L} = \frac{1}{\tau} \tag{5}$$

Where, c is the speed of light, n_{eff} is effective refractive index of fiber. Actually, FSR is related to fiber length, which is an important parameter in ARW model and will be derived.

Since the parameters involved in the experiment are optimized, the specific parameters after optimization will be shown in the experimental part.

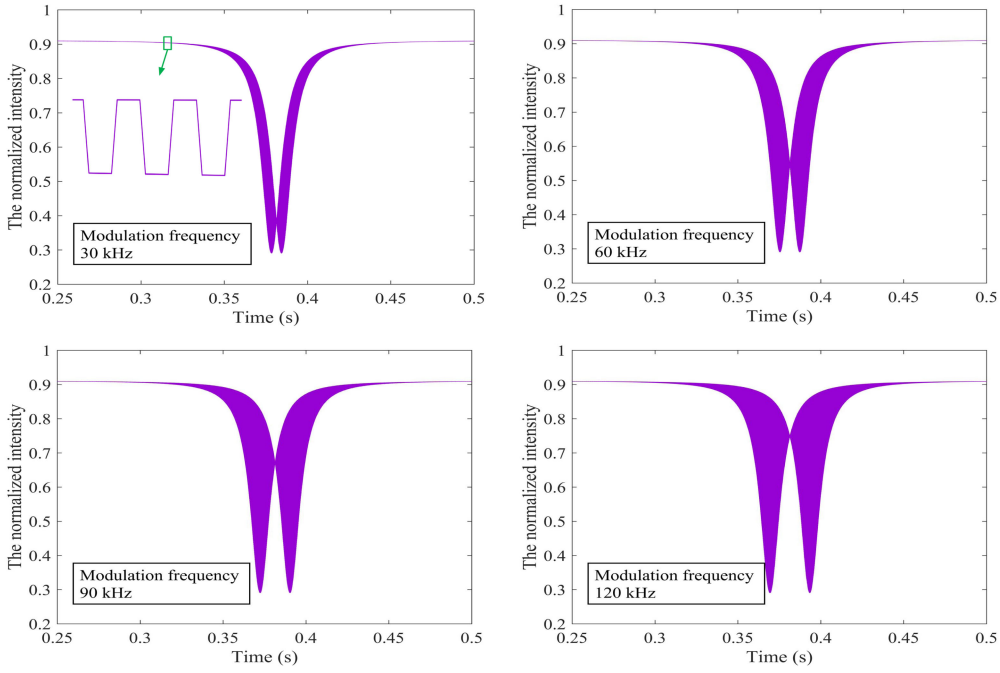

Fig. 3. The effect of different modulation frequency on the resonance phenomenon.

2.2 Demodulation Sensitivity Model

Triangular wave modulation has been widely used in signal processing of RFOG due to its stability and simplicity. The signal detection mechanism of triangular wave modulation is introduced below. For the $LiNbO_3$ phase modulator, although it can't directly shift the optical frequency like the acousto-optic modulator, we can achieve the equivalent frequency shift of the light wave by applying a linear modulation signal. The optical field modulated by the $LiNbO_3$ phase modulator can be expressed as:

$$E_{in\_tri} = E_0 e^{j\{\omega t+\phi(t)+\Delta f t+\frac{2V_p}{V_\pi}\arcsin[\sin(2\pi f t)]\}} \tag{6}$$

In Eq. (6), Δf is a small scanning frequency that is linear with time, f and V_p are modulation frequency and amplitude of triangular wave respectively, V_π is half-wave voltage of phase modulator. In the experiment, the V_π of both phase modulators is 4 V. $\frac{2V_p}{V_\pi}\arcsin[\sin(2\pi f t)]$ is the modulation phase of triangular wave, and its derivative $\frac{2V_p}{V_\pi} f \mathrm{sgn}[\cos(2\pi f t)]$ is the equivalent frequency shift of triangular wave, which is a square wave. According to Eq. (4), the normalized output modulated by triangular wave is:

$$H_{tri} = (1-\alpha_c)\left[1-\rho\cdot\frac{(1-Q)^2}{(1-Q)^2+4Q\sin^2\left(\pi\tau\{\Delta f+\frac{2V_p}{V_\pi} f\,\mathrm{sgn}[\cos(2\pi f t)]\}\right)}\right] \tag{7}$$

The triangular wave demodulation output can be expressed as:

$$\begin{aligned} D_{out} &= H_{tri\_\max} - H_{tri\_\min} \\ &= (1-\alpha_c)\left[\frac{\rho(1-Q)^2}{(1-Q)^2+4Q\sin^2\left(\pi\tau\Delta f-\frac{2\pi f\tau V_p}{V_\pi}\right)}-\frac{\rho(1-Q)^2}{(1-Q)^2+4Q\sin^2\left(\pi\tau\Delta f+\frac{2\pi f\tau V_p}{V_\pi}\right)}\right] \end{aligned} \tag{8}$$

Fig. 3 and 4 show the normalized output of triangular modulation and demodulation. From the magnified view of Fig. 3, it can be found that the resonance phenomenon modulated by the triangular wave is indeed square waves. The effect of different modulation frequencies on the resonance phenomenon is shown in Fig. 3. As the modulation frequency increases, the resonant phenomenon becomes thicker and thicker. Demodulation curves at different modulation frequencies are shown

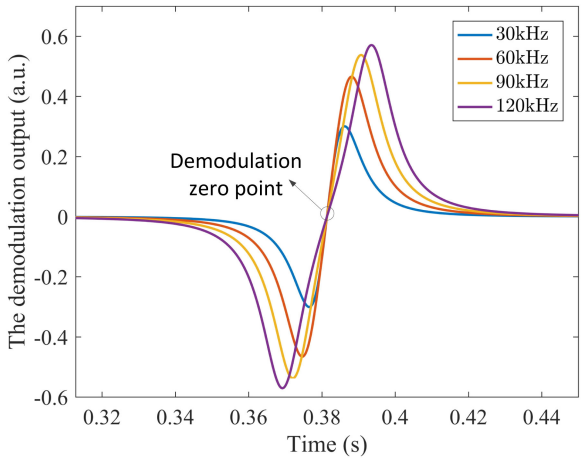

Fig. 4. Demodulation curves at different modulation frequency.

in Fig. 4. The middle region of demodulation curve as shown in figure is almost linear, which is the working area of RFOG. The slope of the working area in the demodulation curve represents the demodulation sensitivity, which is closely related to the error. From the figure, different modulation frequency produces different demodulation sensitivity. Due to the approximate linearity, we replace the slope of demodulation working area with the slope at demodulation zero point:

$$k_0 = \frac{dD_{out}}{d\Delta F}\Big|_{\Delta F=0} = \frac{4\pi\tau Q\rho(1-\alpha_c)(1-Q)^2\sin\left(\frac{4\pi f\tau V_p}{V_\pi}\right)}{\left[(1-Q)^2+4Q\sin^2\left(\frac{2\pi f\tau V_p}{V_\pi}\right)\right]^2} - \frac{4\pi\tau Q\rho(1-\alpha_c)(1-Q)^2\sin\left(-\frac{4\pi f\tau V_p}{V_\pi}\right)}{\left[(1-Q)^2+4Q\sin^2\left(-\frac{2\pi f\tau V_p}{V_\pi}\right)\right]^2} \tag{9}$$

The sensitivity model of demodulation voltage is derived from the Eq. (9):

$$V' = RR_{pd}I_0k_0 \tag{10}$$

Where, R is the photodetector cross-resistance, R_{pd} is the conversion coefficient of photodetector, I_0 is light intensity from the laser.

2.3 ARW Model

In this study, three white noises are taken into account to build ARW model including shot noise, thermal noise and relativity intensity noise. The noises induced by Rayleigh backscattering and other noise source are ignored because their orders of magnitude are relatively small [23], [24]. The generation mechanisms of the three main white noises in RFOG are different, which means that each noise is an independent random noise. Therefore, the system error is the error sum of each noise. The following is the establishment of error models.

- Shot noise model
  Shot noise is a kind of random noise that is generated in the process of converting photons into electrons. For photodetectors, the current standard deviation generated by shot noise can be expressed as:

$$\sigma_{I\_S} = \sqrt{2eI_0H_{\max}R_{pd}B} \tag{11}$$

  Where, e is the electronic power, B is the detection bandwidth. In RFOG, the larger optical power received by the photodetector, the larger shot noise. Therefore, when the maximum light intensity of the resonator reaches the photodetector, the current standard deviation of the shot noise is the largest. $H_{\max}$ is maximum of Eq. (7). Therefore, Eq. (11) represents the largest error. Corresponding variance of demodulation voltage error is:

$$\sigma_S^2 = (\sigma_{I\_S}R)^2 = 2eI_0H_{\max}R_{pd}BR^2 \tag{12}$$

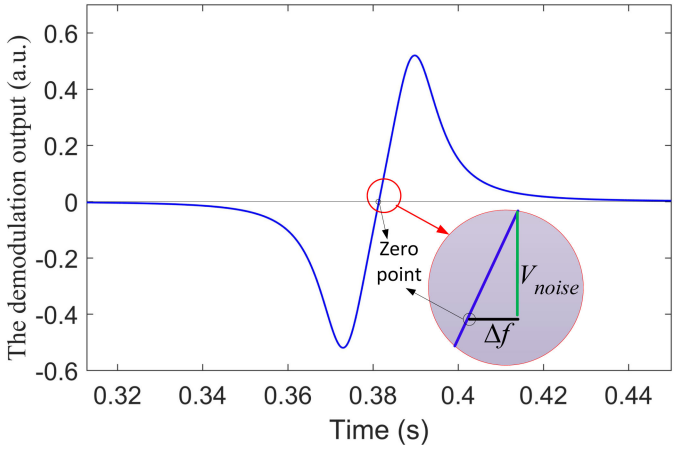

Fig. 5. Diagram of the demodulation error caused by white noises.

- Thermal noise model
  The thermal noise is derived from the Johnson thermal noise of the feedback resistor of the detector's transimpedance amplifier. [25]. Current standard deviation caused by it can be expressed as:

$$\sigma_{I\_T} = \sqrt{4kTB/R} \tag{13}$$

  Where, T is the temperature. Corresponding variance of demodulation voltage error is:

$$\sigma_T^2 = (\sigma_{I\_T} R)^2 = 4kTBR \tag{14}$$

- Relative intensity noise model
  The relative intensity noise (RIN) is the random beat frequency between the uncorrelated frequency components of the light source, causing the power fluctuation [26]. According to [27], the relative intensity noise of laser is defined as:

$$RIN = 10 \log \left\{ \frac{1}{B} \frac{\sigma_{I\_R}^2}{I^2} \right\} \tag{15}$$

  According to the test results of the experimental fiber laser, $RIN = 120$ dB. Current standard deviation can be expressed as:

$$\sigma_{I\_R} = I_0 H_{\max} R_{pd} \sqrt{B} \times 10^{-6} \tag{16}$$

  Corresponding variance of demodulation voltage error is:

$$\sigma_R^2 = R^2 B \sigma_{I\_R}^2 \tag{17}$$

Fig. 5 shows the principle of demodulation error generated by white noise. Each noise corresponds to a demodulation voltage error. Therefore, the demodulation frequency error can be calculated by the voltage error expressed by a green line and demodulation voltage sensitivity. Each of three noises is independent. They are superimposed at the demodulation zero, which is the essential cause of the noise-induced demodulation error. Therefore, the demodulation frequency errors corresponding to the above three noises can be expressed respectively. Demodulation frequency error induced by shot noise:

$$\Delta f_S = \sqrt{(\sigma_S / V')^2} \tag{18}$$

Demodulation frequency error induced by thermal noise:

$$\Delta f_T = \sqrt{(\sigma_T / V')^2} \tag{19}$$

Demodulation frequency error induced by RIN:

$$\Delta f_R = \sqrt{(\sigma_R / V')^2} \tag{20}$$

The noise performance of the gyro depends on the signal-to-noise ratio (SNR) of the system, and the theoretical SNR in RFOG system is expressed as [20]:

$$SNR = \left(\frac{V'}{\sqrt{{\sigma_{sv}}^2 + {\sigma_{hv}}^2 + {\sigma_{RIN}}^2}} \right)^2 = \left(\frac{1}{\sqrt{{\Delta f_S}^2 + {\Delta f_T}^2 + {\Delta f_R}^2}} \right)^2 \tag{21}$$

Considering the relationship between ARW and SNR, the ARW model is built:

$$ARW = \frac{1}{\sqrt{SNR}} \frac{n_{eff}\lambda}{D} \tag{22}$$

Where, $\frac{n_{eff}\lambda}{D}$ is the reciprocal of scale factor, n_{eff} is effective refractive index of fiber, λ is central wavelength of laser, D is diameter of resonator.

Submitting Eq. (10) to Eq. (21) into Eq. (22):

$$ARW = \frac{n_{eff}\lambda \sqrt{2el_0 H_{\max} R_{pd} B + 4kTB + B^2 {I_0}^2 {H_{\max}}^2 {R_{pd}}^2 \times 10^{-12}}}{D R_{pd} I_0 k_0} \tag{23}$$

Eq. (23) is the final established ARW model, and the main system parameters are all included in this formula. Based on this formula, multi-parameter optimization and modulation frequency optimization are performed.

3. Optimization

The relative variation of ARW, rather than the absolute variation, is applied in simulation and experiment to highlight the trend of ARW, thus demonstrating the effectiveness of modulation frequency optimization. The influences of main system parameters on ARW at different modulation frequencies are simulated first. The approximate range of each parameter is determined based on simulation results and actual factors. Then the range of each parameter is used as the optimization range of the PSO algorithm. After the algorithm operation, the set of optimal parameters for minimizing ARW is found. Finally, we apply this set of parameters in experiment system and obtain the experimental results that are basically consistent with simulation.

3.1 Parameters Analysis

Fig. 6 shows the relative increase of ARW and SNR with modulation frequency. By observing the curve, it is found that the reasonable selection of modulation frequency effectively increase SNR and improve ARW. So the feasibility of this method can be further analyzed. Five important system parameters, namely, coupling coefficient, coupler loss, fiber length, fiber loss, and laser linewidth are analyzed with different modulation frequencies, as shown in Fig. 6. The purpose of this process is to lay the foundation for final parameter optimization.

Fig. 7 simulates the relative increase of ARW of different parameters with modulation frequency. According to Fig. 7(a), as the coupling coefficient increases, the ARW has a tendency to decrease first and then increase. And there will be a corresponding modulation frequency for different coupling coefficient, making the ARW minimum. Fig. 7(b) shows the influence of coupler loss on ARW. It can be found from the simulation that increased coupler loss causes ARW to increase at the same time. However for each fixed loss value, there is a corresponding optimal modulation frequency to minimize ARW. And the larger loss, the higher optimal modulation frequency. According to Fig. 7(c), the increase of the fiber length makes the ARW have a decreasing trend. But our previous research [28] has shown that the increase of fiber length would cause the resonator to generate

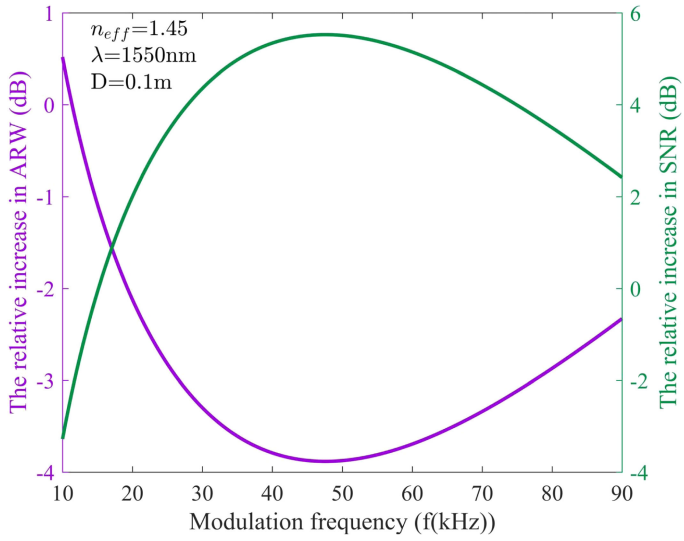

Fig. 6. The relative increase in ARW and SNR.

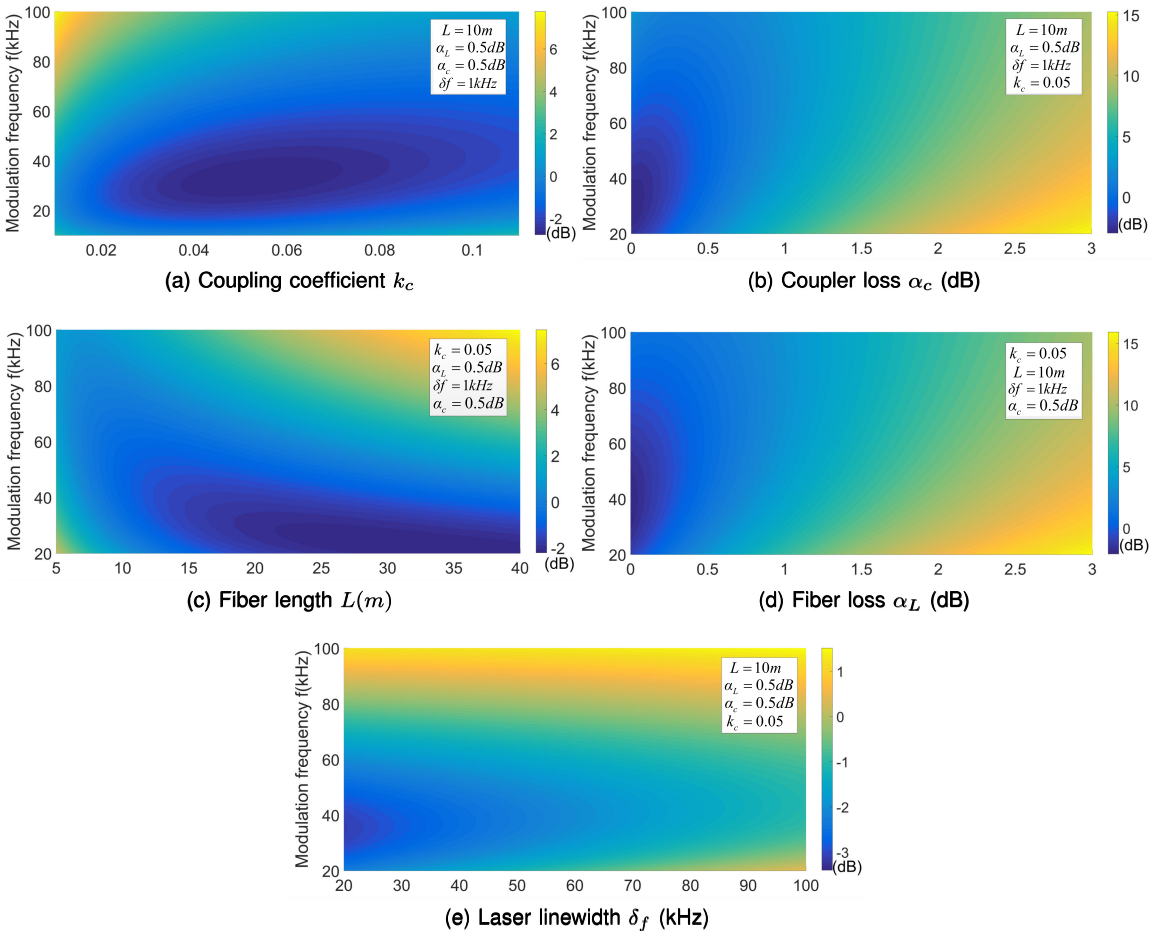

Fig. 7. The relative increase in ARW under different parameters.

overshoot, and increase the difficulty of signal processing. So the fiber length cannot be added wirelessly. Through simulation, it can also be seen that for each fixed fiber length, there will also be a modulation frequency minimizing the ARW. Fig. 7(d) shows that resonator fiber loop loss and coupler loss have similar effects on ARW, so the analysis process is similar to Fig. 7(b). Fig. 7(e) shows that the decrease of laser linewidth is beneficial to improve the ARW. For a fixed linewidth, an optimal modulation frequency can also be found to minimize the ARW. Therefore, it is meaningful to choose modulation frequency reasonably for lasers with different linewidths in system.

3.2 Particle Swarm Optimization

The above analysis is only a trend of certain parameter. However, since the parameters can affect each other, comprehensive optimization of multiple parameters is required when selecting specific values. The PSO algorithm has the advantages of multi-parameter optimization, fast calculation speed and high accuracy. Therefore, this algorithm is used to optimize the multi-parameters, so as to select a set of system parameters that make the ARW lowest.

PSO algorithm is used to optimize the above-mentioned five important system parameters and modulation frequency at the same time. First, the allowable application range of each parameter is set according to above simulation results. Then the algorithm finds the lowest ARW and gives the corresponding set of optimal parameters.

Fig. 8 is a flow chart of the PSO algorithm. At the beginning of the algorithm, a group of random particles is initialized. Since there are six parameters, all particles are in a six-dimensional space. Each particle represents a position in a six-dimensional space. Initialization includes velocity, position, fitness of particle. Then they update their speed V and position X according to the following two formulas:

$$\begin{aligned} V_k(f, k_c, \alpha_c, L, \alpha_L, \delta f) = {} & \omega \times V_{k-1}(f, k_c, \alpha_c, L, \alpha_L, \delta f) \\ & + c_1 \times rand \times [pBest - X_{k-1}(f, k_c, \alpha_c, L, \alpha_L, \delta f)] \\ & - c_2 \times rand \times [gBest - X_{k-1}(f, k_c, \alpha_c, L, \alpha_L, \delta f)] \end{aligned} \tag{24}$$

$$X_k(f, k_c, \alpha_c, L, \alpha_L, \delta f) = X_{k-1}(f, k_c, \alpha_c, L, \alpha_L, \delta f) + V_k(f, k_c, \alpha_c, L, \alpha_L, \delta f) \tag{25}$$

where ω is the inertia factor. c_1, c_2 are the learning factors. $pBest$ is the individual extremum, which is the optimal solution found by each particle. $gBest$ is the global extremum indicating the optimal solution found by the entire particle swarm. $rand$ represents a random number, the initial range of each parameter can be determined by this value. After the information is updated, the particles iteratively find the optimal solution. In each iteration, the particle updates itself by tracking $pBest$ and $gBest$. If the ARW value of the current position is smaller than that of the $pBest$ position, the current position is taken as $pBest$. If the ARW value of the $pBest$ position is smaller than that of the $gBest$ position, the $pBest$ position is taken as $gBest$. When the ARW at $gBest$ is within the set accuracy range, then the ARW and $gBest$ are output, and the algorithm ends. Otherwise, the program jumps to the front to start the iteration again.

Table 1 shows the choosing range and optimal result using PSO. It is found from Table I that the coupler loss, fiber loss, laser linewidth are positively correlated with ARW. Fiber length is negatively correlated with ARW. The optimal coupling coefficient is found to minimize ARW. The above results are in good agreement with the simulation results in Fig. 7, further verifying the correctness of the PSO algorithm.

4. Experimental Work

4.1 Experimental Setup

The signal detection process is closely related to the error induced by white noise. Therefore the signal flow of RFOG will be introduced first. The Fig. 9 shows the schematic diagram of RFOG system based on the $LiNbO_3$ phase modulator, which can be divided into optical path

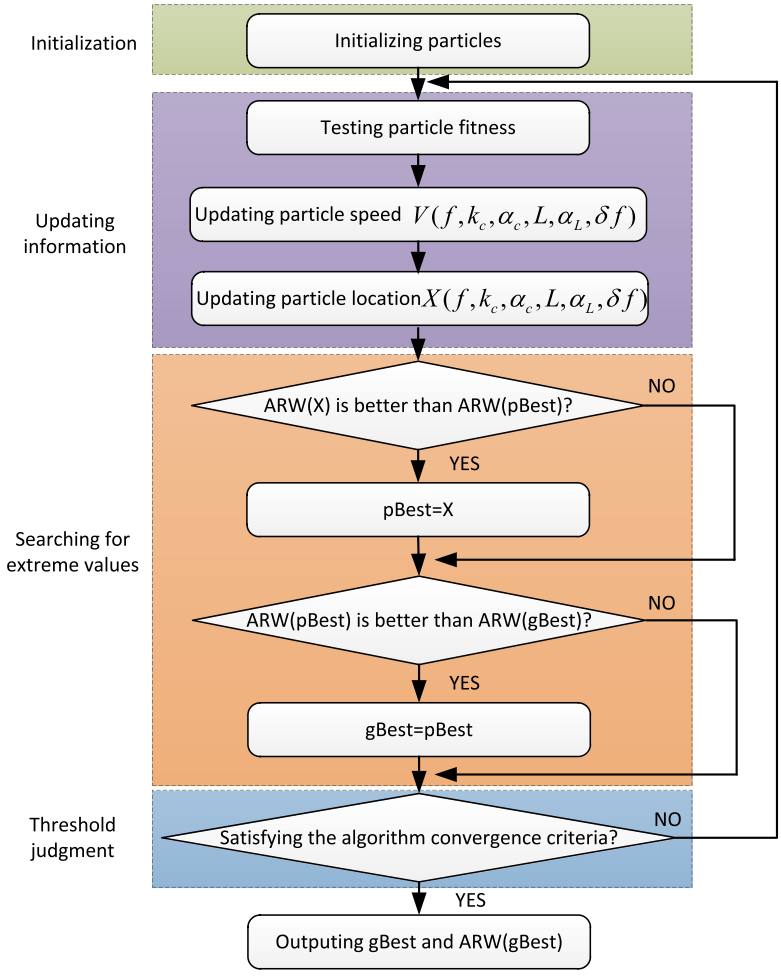

Fig. 8. PSO algorithm framework diagram.

TABLE 1
THE CHOOSING RANGE AND OPTIMAL RESULT USING PARTICLE SWARM OPTIMIZATION

Parameter	Choosing range	Optimal result
Modulation frequency	$10-100kHz$	$65kHz$
Coupling coefficient	$0.01-0.5$	0.05
Coupler loss	$0.5-3dB$	$0.5dB$
Fiber length	$1-10m$	$10m$
Fiber loss	$0.5-3dB$	$0.5dB$
Laser linewidth	$1-100kHz$	$1kHz$

and circuit section. The optical path mainly includes a continuous-wave laser, which is a fiber laser manufactured by NKT Photonics Inc. with a linewidth of less than 1 kHz. The output power in the experiment is about 5 mw. The optical path also includes a 50:50 split ratio coupler, two $LiNbO_3$ straight waveguide phase modulators, two fiber circulators and a reflective fiber resonator. It should be noted that in order to suppress the polarization fluctuation noise, all the optic fiber devices in Fig. 9 are polarization-maintaining, working at 1550 nm. The circuit section, powered by ± 5 V DC regulated power supply, mainly completes the functions of modulation signal generation,

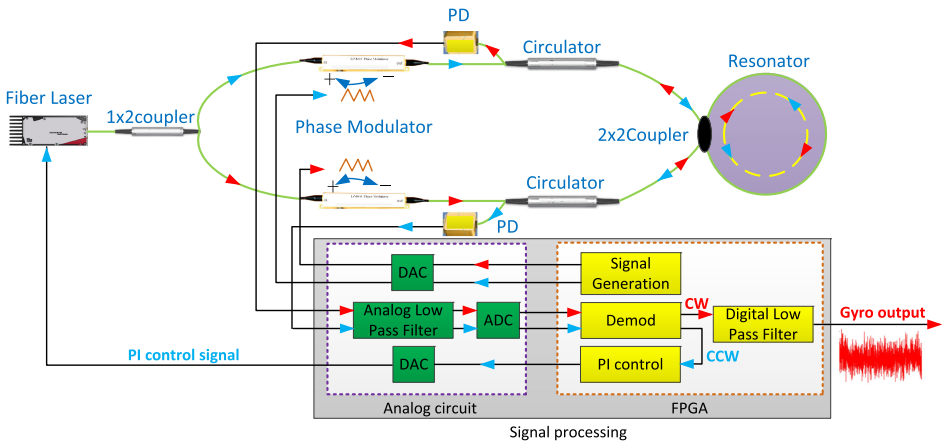

Fig. 9. Diagram of the experimental RFOG system.

phase-locked amplification and demodulation, gyro signal output and proportional integral (PI) control digital feedback. The photodetector acts as a bridge between optical path and circuit part to complete the photoelectric signal conversion.

In the Fig. 9, green lines represent light signal and black lines represent electricity signal. The red arrows direct the clockwise (CW) signal flow direction of resonator, while the blue arrows direct the counterclockwise (CCW) direction. The light from narrow linewidth laser passes through a 3 dB coupler and is split into two beams. Each beam is modulated by $LiNbO_3$ phase modulator. The triangular wave is generated by Field-Programmable Gate Array (FPGA). The modulated signal enters the resonator for transmission, and multiple beam interference occurs at the output port of 2×2 coupler. This part has been described in detail when modeling the resonator. The output light of resonator reaches the photodetector via circulator, and then enters the signal processing circuit for filter and demodulation. Finally, the output frequency of laser is adjusted according to CCW demodulated signal to lock it at the CCW resonant frequency through the PI control loop. The CW signal is directly output as gyro output after demodulation. The gyro output data is observed by an oscilloscope and stored in a digital form in a computer. The experiment was done at room temperature of 25 degrees Celsius.

4.2 Experimental Results

After optimizing the system parameters by the PSO algorithm, the set of optimization parameters listed in Table 1 is applied to the experimental system. In order to verify the significance of modulation frequency optimization, the modulation frequency is changed under the premise that other system parameters are unchanged. In the experiment, the CW and CCW modulation frequencies are set to have small differences to suppress backscattering noise. Three different sets of modulation frequencies are applied in the system, which are CW 19 kHz, CCW 21 kHz and CW 60 kHz, CCW 61 kHz and CW 99 kHz, CCW 101 kHZ respectively.

Three sets of experimental gyro output and fitted Allan deviation results are shown in the Fig. 10. Data for each group of experiments is collected for 1200 seconds. It can be clearly seen from the figure that the gyro output amplitude is gradually smaller when the modulation frequency is from 21 kHz to101 kHz and then to 61 kHz. And the ARW has a significant improvement, the smallest Allan variance is reduced from 2 mV to 1 mV. This trend is consistent with the simulation results of Fig. 6. However, in the experiment, the minimum ARW corresponds to a modulation frequency of 61 kHz, which is different from the simulation. After analysis, the reason why there is a difference between simulation and experiment can be obtained from two aspects. For fiber devices, the fiber loss and coupler loss are higher than the simulation values. On the other hand, other white noises

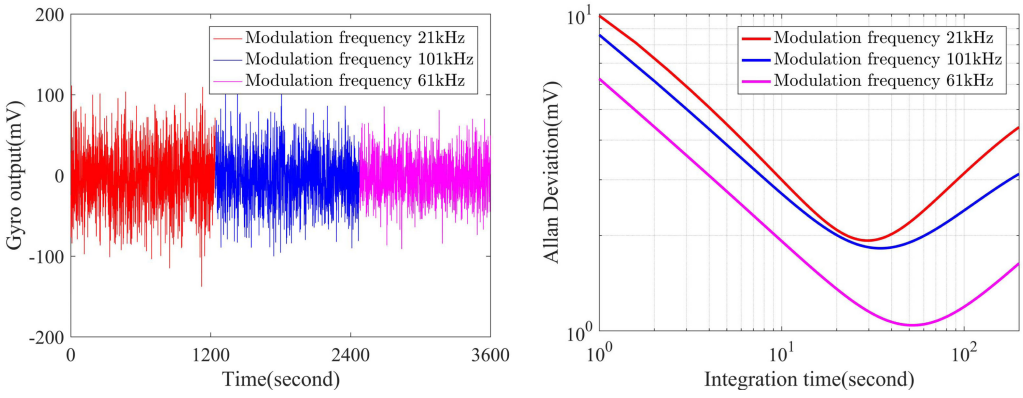

(a) Gyro output (b) Fitted Allan deviation

Fig. 10. Gyro output and fitted Allan deviation with different modulation frequency.

ignored in model also weaken the improvement of ARW to some extent. For the numerical analysis, standard deviation of gyro output voltage reduced by 1.4 dB from 2.5 mV to 1.8 mV when the modulation frequency is 61 kHz compared with the 21 kHz. At the same time, ARW is improved by nearly 2 dB from 1.7 mV/$\sqrt{\text{h}}$ to 1.1 mV/$\sqrt{\text{h}}$. According to Eq. 10, the demodulation voltage sensitivity improved from 1.1 mV/kHz to 1.6 mV/kHz. The experimental results show that the method of optimizing modulation frequency can improve ARW and realize white noise suppression effectively.

5. Conclusion

In this paper, the ARW of RFOG is analyzed and modeled based on the signal processing principle.The optimization method of modulation frequency for reducing ARW is proposed. Then the influences of important system parameters on ARW are analyzed respectively. Parameter selection is performed using PSO algorithm to minimize ARW. Finally, it is verified by experiments that appropriate selection of modulation frequency can improve ARW and reduce the influence of white noise on RFOG effectively.

Acknowledgment

The authors wish to thank the anonymous reviewers for their valuable suggestions.

References

[1] B. R. Johnson, E. Cabuz, H. B. French, and R. Supino, "Development of a MEME gyroscope for northfinding applications," in *Proc. IEEE/ION Position Location Navigation Symp.*, 2010, pp. 168–170.
[2] W. Chow, J. Gea-Banacloche, L. Pedrotti, V. Sanders, W. Schleich, and M. Scully, "The ring laser gyro," *Rev. Modern Phys.*, vol. 57, no. 1, pp. 61–104, 1985.
[3] C. Ciminelli *et al.*, "A high-Q InP resonant angular velocity sensor for a monolithically integrated optical gyroscope," *IEEE Photon. J.*, vol. 8, no. 1, Feb. 2016, Art. no 6800418.
[4] H. C. Lefèvre, *The Fiber-Optic Gyroscope*, 2nd ed. Norwood, MA, USA: Artech House, 2014.
[5] H. Ma, Y. Yan, Y. Chen, and Z. Jin, "Improving long-term stability of a resonant micro-optic gyro by reducing polarization fluctuation," *IEEE Photon. J.*, vol. 4, no. 6, pp. 2372–2381, Dec. 2012.
[6] X. Li, J. Zhang, H. Ma, and Z. Jin, "Test and analysis of the optical Kerr-effect in resonant micro-optic gyros," *IEEE Photon. J.*, vol. 6, no. 5, 2014, Art. no. 6601007.
[7] J. Nayak, "Fiber-optic gyroscopes: from design to production [invited]," *Appl. Opt.*, vol. 50, no. 25, pp. E152–E161, 2011.
[8] R. Bergh, H. Lefevre, and H. Shaw, "An overview of fiber-optic gyroscopes," *J. Lightw. Technol.*, vol. 2, no. 2, pp. 91–107, Apr. 1984.

[9] H. C. Lefvre, "The fiber-optic gyroscope: Challenges to become the ultimate rotation-sensing technology," *Opt. Fiber Technol.*, vol. 19, no. 6, pp. 828–832, 2013.
[10] R. E. Meyer, S. Ezekiel, D. W. Stowe, and V. J. Tekippe, "Passive fiber-optic ring resonator for rotation sensing," *Opt. Lett.*, vol. 8, no. 12, pp. 644–646, 1983.
[11] Z. Li, N. He, X. Sun, C. Jin, C. Liu, and X. Wu, "Analysis of resonance asymmetry phenomenon in resonant fiber optic gyro," *Sensors*, vol. 18, no. 3, 2018, Art. no. E696.
[12] Z. Jin, X. Yu, and H. Ma, "Resonator fiber optic gyro employing a semiconductor laser." *Appl. Opt.*, vol. 51, no. 15, pp. 2856–2864, 2012.
[13] X. Jin, Y. Lin, Y. Lu, H. Ma, and Z. Jin, "Short fiber resonant optic gyroscope using the high-frequency Pound-Drever-Hall technique," *Appl. Opt.*, vol. 57, no. 20, pp. 5789–5793, 2018.
[14] N. He *et al.*, "Temperature stability of a hybrid polarization-maintaining photonic crystal fiber resonator and its application in a resonant fiber optic gyro," *Sensors*, vol. 18, no. 8, 2018, Art. no. 2506.
[15] H. Jiao, L. Feng, N. Liu, and Z. Yang, "Improvement of long-term stability of hollow-core photonic-crystal fiber optic gyro based on single-polarization resonator," *Opt. Exp.*, vol. 26, no. 7, pp. 8645–8655, 2018.
[16] H. Jiao, L. Feng, K. Wang, N. Liu, and Z. Yang, "Analysis of polarization noise in transmissive single-beam-splitter resonator optic gyro based on hollow-core photonic-crystal fiber," *Opt. Exp.*, vol. 25, no. 22, pp. 27806–27817, 2017.
[17] H. Jiao, L. Feng, J. Wang, K. Wang, and Z. Yang, "Transmissive single-beam-splitter resonator optic gyro based on a hollow-core photonic-crystal fiber," *Opt. Lett.*, vol. 42, no. 15, pp. 3016–3019, 2017.
[18] K. M. Killian, M. Burmenko, and W. Hollinger, "High-performance fiber optic gyroscope with noise reduction," *Proc. SPIE*, vol. 2292, pp. 255–264, 1994.
[19] A. Noureldin, D. Irvine-Halliday, H. Tabler, and M. P. Mintchev, "New technique for reducing the angle random walk at the output of fiber optic gyroscopes during alignment processes of inertial navigation systems," *Opt. Eng.*, vol. 40, no. 10, pp. 2097–2107, 2001.
[20] G. A. Pavlath, "Method for reducing random walk in fiber optic gyroscopes," U.S. Patent 5,530,545, Jun. 25, 1996.
[21] Z. Jiang, Z. Hu, and C. Fu, "Angular random walk limited by Rayleigh backscattering in resonator fiber optic gyros." *Appl. Opt.*, vol. 56, no. 34, pp. 9414–9422, 2017.
[22] M. A. Guillén-Torres, E. Cretu, N. A. F. Jaeger, and L. Chrostowski, "Ring resonator optical gyroscopes—Parameter optimization and robustness analysis," *J. Lightw. Technol.*, vol. 30, no. 12, pp. 1802–1817, Jun. 2012.
[23] C. C. Cutler, S. A. Newton, and H. J. Shaw, "Limitation of rotation sensing by scattering," *Opt. Lett.*, vol. 5, no. 11, pp. 488–490, 1980.
[24] K. Takada, "Calculation of Rayleigh backscattering noise in fiber-optic gyroscopes," *J. Opt. Soc. Amer. A*, vol. 2, no. 6, pp. 872–877, 1985.
[25] P. F. Wysocki, M. J. F. Digonnet, and B. Y. Kim, "Broad-spectrum, wavelength-swept, erbium-doped fiber laser at 1.55 μm," *Opt. Lett.*, vol. 15, no. 16, pp. 879–881, 1990.
[26] P. F. Wysocki, M. J. F. Digonnet, and B. Y. Kim, "Wavelength stability of a high-output, broadband, Er-doped superfluorescent fiber source pumped near 980 nm," *Opt. Lett.*, vol. 16, no. 12, pp. 961–963, 1991.
[27] S. D. Dyer and K. B. Rochford, "Spectral tailoring of erbium superfluorescent fibre source," *Electron. Lett.*, vol. 34, no. 11, pp. 1137–1139, 1998.
[28] Z. Wang, G. Wang, W. Gao, Z. Wang, Z. Wang, and W. Miao, "Resonator optimization of the resonant fiber optic gyro under dynamic condition," in *Proc. IEEE/IOn Position Location Navigation Symp.*, 2018, pp. 31–33.